40th Fluid Dynamics Conference and Exhibit
28 June - 1 July 2010, Chicago, Illinois

AIAA 2010-4714

# Effects of Distributed Suction on an Airfoil at Low Reynolds Number

Redha Wahidi[1] and David H. Bridges[2]
*Department of Aerospace Engineering, Mississippi State University, MS 39762*

**A suction distribution was designed based on Thwaites' criterion of separation. The effectiveness of the designed suction distribution in controlling the size of the laminar separation bubble on a LA2573a airfoil was investigated. The suction distribution was capable of maintaining an unseparated laminar boundary up to the original transition location. The effects of applying different suction rates on the drag were tested. Drag reductions between 14 and 24 % were achieved. The penalty for utilizing suction was estimated by introducing an equivalent suction drag. The analysis showed that the penalty for using suction to reduce the drag was relatively small.**

**Nomenclature**

| | | |
|---|---|---|
| $AoA$ | = | alpha = $\alpha$ = angle of attack |
| $b$ | = | span of the airfoil |
| $c$ | = | local wing chord |
| $C_d$ | = | drag coefficient |
| $C_Q$ | = | suction coefficient |
| $d_h$ | = | suction hole diameter |
| $H$ | = | shape factor [$\delta^*/\theta$] |
| $k$ | = | discharge loss coefficient through the holes |
| $M$ | = | number of holes per unit length in the spanwise direction |
| $p_c$ | = | chamber static pressure |
| $p_e$ | = | static pressure at the edge of boundary layer |
| $p_o$ | = | freestream static pressure |
| Q | = | volumetric suction rate |
| $q$ | = | dynamic pressure [ ½ $\rho$ $U_0^2$] |
| $R$ | = | location of reattachment point |
| $Re_c$ | = | Reynolds number based on airfoil chord |
| $S$ | = | location of separation point |
| $T$ | = | location of transition point |
| $u$ | = | longitudinal component of the mean velocity |
| $u_e$ | = | edge velocity |
| $U_0$ | = | freestream velocity |
| $v_h$ | = | velocity through an individual hole |
| $v_w$ | = | wall suction velocity |
| $x$ | = | direction along the surface of the airfoil |
| $x/c$ | = | direction along the chord of the airfoil normalized by the chord |
| $\Delta x$ | = | surface distance between holes in the chordwise direction |
| $\Delta y$ | = | surface distance between holes in the spanwise direction |
| $\delta^*$ | = | boundary layer displacement thickness |

[1]Lecturer, Department of Aerospace Engineering, P. O. Drawer A.
[2]Associate Professor, Department of Aerospace Engineering, P. O. Drawer A, Associate Fellow, AIAA

$\lambda$ = Thwaites pressure gradient parameter
$\mu$ = viscosity of air
$\nu$ = kinematic viscosity of air
$\theta$ = boundary layer momentum thickness
$\rho$ = density of air
$\tau_w$ = wall shear stress

## I. Introduction

Flow separation on the surface of an airfoil causes a significant increase in drag. If the separated boundary layer fails to reattach on the surface of the airfoil, a complete loss of lift and dramatic increase in drag results. If the separated boundary layer reattaches to the surface of the airfoil, a laminar separation bubble (LSB) exists on the airfoil. For low Reynolds number flows, typically $10^4 < Re < 10^6$, the boundary layer is laminar over a significant portion of the airfoil. The laminar boundary layer separates when it encounters an adverse pressure gradient. A separated shear layer develops downstream of the separation point, over which the disturbances in the flow grow to a critical value and the flow transitions to turbulence. The turbulence level downstream of the transition in the shear layer becomes higher and a larger amount of fluid is entrained. The entrainment of fluid causes the necessary pressure rise for reattachment. The flow achieves this bubble pressure recovery (*i.e.* the pressure necessary to equate the surface pressure distribution to that of an inviscid solution, see Crabtree (1959)) by the continuous rise of pressure along the wall which may extend downstream of the reattachment point.

The LSB causes an increase in drag and is susceptible to bursting if the angle of attack is increased or the Reynolds number is decreased. Therefore, it is desirable to control the LSB in order to reduce the drag and prevent it from bursting. The bubble could be eliminated by using a transition strip upstream of the location of separation to produce a turbulent boundary layer capable of negotiating the adverse pressure gradient. However, the turbulent boundary layer produces higher skin friction drag than the laminar boundary layer. Also, the position of the transition strip is fixed on the surface of the airfoil which means that it must be fixed at the most forward location of any predicted separation location. This would cause an earlier-than-required transition location at moderate angles of attack. The application of suction to prevent separation and delay transition is very effective; however, the cost of applying suction could be much higher than the drag reductions obtained from eliminating separation and delaying transition. Therefore, the ideal approach would be to reduce the drag associated with flow separation without increasing the skin-friction drag. This goal could be achieved by applying boundary layer suction over the forward portion of the bubble between the separation and transition locations to maintain an unseparated laminar boundary layer without changing the location of transition. Another benefit that could be achieved by applying suction over a very small area is that the suction requirements would be small which would reduce the penalties associated with the application of suction. The effectiveness of applying boundary layer suction only to maintain an unseparated laminar boundary layer between the original separation and transition locations without significantly changing the original transition location is investigated in this study.

A distributed suction was designed based on Thwaites' criterion of separation (see White (2005) for more details on Thwaites method). The effect of the distributed suction on the size of the LSB was investigated by carrying out boundary layer velocity measurements. The effects on the drag of different suction distributions and suction rates were investigated at different angles of attack at $Re_c$ = 250,000.

## II. Suction Design

### A. Thwaites Method

Thwaites method is a one-parameter integral method for predicting integral properties of laminar boundary layers. If the inviscid or edge velocity $u_e$ is known as a function of distance along the airfoil surface, measured from the stagnation point, then the momentum thickness ($\theta$) may be found from the integral relation as shown in Eq.(1):

$$\theta^2(x) = \frac{0.45\nu}{u_e^6}\int_0^x u_e^5\, dx' \tag{1}$$

Thwaites pressure gradient parameter $\lambda(x)$ is defined as in Eq. (2):

$$\lambda(x) = \frac{\theta^2(x)}{\nu}\frac{du_e}{dx} \tag{2}$$

This parameter may then be used with a correlation $S(\lambda)$ to compute the wall shear stress from Eq. (3) as follows:

$$\tau_w(x) = \frac{\mu u_e(x)}{\theta(x)} S(\lambda) \tag{3}$$

White (2005) recommends a correlation of the form:

$$S(\lambda) = (\lambda + 0.09)^{0.62} \tag{4}$$

Plotting the shape factors for different exact laminar boundary layer solutions against Thwaites parameter ($\lambda$) shows that the shape factor $H(\lambda)$ is a universal function. White (2005) recommends a correlation for the shape factor $H(\lambda)$, using the intermediate variable $z = (0.25 - \lambda)$ as shown in Eq. (5)

$$H(\lambda) = 2.0 + 4.14z - 83.5z^2 + 854z^3 - 3337z^4 + 4576z^5 \tag{5}$$

Thwaites, in his compilation of data that led to his integral, found that laminar boundary layer separation was correlated well by a value of $\lambda = \lambda_{sep} = -0.09$.

The accuracy of Thwaites method in predicting separation was shown by the experimental results of Crabtree (1959) which agreed very well with the locations of separation predicted by the method of Thwaites. With regards to the current study, Fig. (1) shows the $C_p$ results on the LA2573a airfoil at different angles of attack at $Re_c$ = 250,000. The symbols (*S*), (*T*) and (*R*) on the figure designate the separation, transition and reattachment locations obtained from the surface pressure and boundary layer measurements. The figure also shows the separation locations predicted using Thwaites method. The agreement between predicted separation locations and those determined from the experimental results is very good.

**B. Suction Distribution**

The analysis presented in this section provides an optimal suction distribution based on Thwaites method for a given airfoil at a certain angle of attack and Reynolds number. Due to the time and cost associated with building the perforated airfoil models, only one model could be built. Therefore, the analysis was applied at different flow conditions for the LA2573a airfoil and an optimum distribution was determined for each condition. The distribution that was actually used when the model was constructed was an average of these optimum distributions.

The idea for separation prevention presented in this study is as follows. Suppose that $\lambda$ is to be held constant at a value $\lambda_0$ near the separation value $\lambda_{sep} = -0.09$. The definition of $\lambda$ then provides a formula for the momentum thickness:

$$\theta(x) = \sqrt{\frac{\nu\lambda_0}{du_e/dx}}\,, \tag{6}$$

where $u_e(x)$ was obtained from the inviscid solution using XFLR5, which is the "freeware" version of the airfoil analysis program XFOIL. Note from this expression that the signs of $\lambda_0$ and $du_e/dx$ must be the same to avoid imaginary values of the momentum thickness. This means that a negative value of $\lambda_0$ must be chosen in the regions of adverse pressure gradient where $du_e/dx < 0$. If the value of $\lambda_0$ is fixed, then the values of $S(\lambda)$ and $H(\lambda)$ are also fixed through the correlations given in Eqs. (4) and (5), respectively, so that $S = S_0 = S(\lambda_0)$ and $H = H_0 = H(\lambda_0)$. The momentum integral equation may then be rewritten (see Wahidi and Bridges, 2008) to provide the suction velocity distribution necessary to maintain the constant value $\lambda_0$:

$$v_w(x) = \frac{\nu S_0}{\theta(x)} - (2 + H_0)\theta(x)\frac{du_e(x)}{dx} - u_e(x)\frac{d\theta(x)}{dx} \tag{7}$$

It should be noted that this expression assumes a positive suction velocity into the airfoil. Also, in this expression, $x$ is actually the distance along the surface, measured from the forward stagnation point.

The suction velocity distributions provided by Eq. (7), shown in Fig. (2), were compared at $\alpha$ = 2, 4 and 6 degrees at $Re_c$ = 250,000. The suction velocities are normalized by the freestream velocity. The suction in all the cases begins at the value of $x$ where Thwaites method predicts that $\lambda = -0.08$. It is seen

that for the most part, the suction velocities are much less than 1% of the freestream velocity. The effect of varying $\lambda_0$ is shown in Fig. (3). The shapes of the distributions do not generally change with the value of $\lambda$, but the distributions have a greater chordwise extent and an earlier starting point at larger (or less negative) values of $\lambda_0$. The figures show that the less negative value of $\lambda_0$ requires a starting location ($s$) further upstream and a correspondingly larger value of $v_w$ in the vicinity of the starting location ($s$). It therefore appears that the better course is to choose a value of $\lambda_0$ as close to $\lambda_{sep}$ = -0.09 as possible to reduce the required suction.

The suction velocity distributions $v_w(x)$ presented in Fig. 2 are computed as continuous functions. A suction velocity distribution must be converted into a discrete distribution in order to implement it on an actual airfoil. In the following discussion, it will be assumed that the inside of the wing is a single chamber at a single pressure $p_c$ which is lower than the lowest outside pressure. The flow through the surface depends on the difference between the pressure at the edge of the boundary layer, $p_e$ (which comes from the inviscid analysis), and the chamber pressure $p_c$. The total volumetric flow through the surface is assumed to be a sum of the flow through the individual holes. The pressure at a point on the airfoil may be obtained from Bernoulli's equation:

$$p_e + \frac{1}{2}\rho u_e^2 = p_0 + \frac{1}{2}\rho U_0^2 \Rightarrow p_e(x) = p_0 + \frac{1}{2}\rho U_0^2\left[1 - \left(\frac{u_e(x)}{U_0}\right)^2\right] \tag{8}$$

The pressure difference that drives the flow through the hole is then given by

$$p_e(x) - p_c = \Delta p_e(x) = \Delta p_c + \frac{1}{2}\rho U_0^2\left[1 - \left(\frac{u_e(x)}{U_0}\right)^2\right], \quad \Delta p_c = p_0 - p_c \tag{9}$$

Note that in these equations $p_0$ is the freestream static pressure. Equation (9) is constructed such that the difference $p_e(x) - p_c$ is positive. It is then assumed that the velocity through an individual hole is given by

$$v_h = k\sqrt{\frac{2\Delta p_e}{\rho}} \tag{10}$$

In this equation, $k$ is a loss coefficient. It is now assumed that the suction will take place through rows of holes spaced a variable distance $\Delta x$ apart in the chordwise direction over a length $\Delta y$ in the spanwise direction. The hole spacing in the spanwise direction is assumed to be constant, with $M$ being the number of holes per unit distance in the spanwise direction. The total number of holes in a single row in a distance $\Delta y$ in the spanwise direction is then $M\Delta y$. If the distances $\Delta x$ and $\Delta y$ are sufficiently small, then the volumetric flow through a rectangular area $\Delta x\Delta y$ from the continuous suction velocity $v_w$ would be $v_w\Delta x\Delta y$. If a single row of holes spaced $\Delta x$ from the next row is supposed to produce the same volumetric flow rate though the same area, then equating the volumetric flow rates yields

$$v_w(x)\Delta x\Delta y = M\Delta y v_h \frac{\pi}{4}d_h^2 \;\Rightarrow\; \Delta x(x) = \frac{\pi}{4v_w(x)}Md_h^2 v_h \tag{11}$$

In this equation $d_h$ is the suction hole diameter and the hole velocity $v_h$ is given by Eq. (10). The suction velocity $v_w(x)$ is defined by Eq. (7).

The suction distribution obtained by Thwaites method is only optimal at a certain angle of attack and at a certain Reynolds number. This distribution may present difficulties in controlling the boundary layer at other flow conditions. Also, the required spacing distances in the high curvature region on the airfoil produced by the above analysis were very small. These small distances between the suction rows are difficult to perforate and they could affect the integrity of the structure of the airfoil. Therefore, a more-reasonable spacing from a construction point of view was selected. Additionally, since the purpose of using suction in this research is to develop a generic distribution that can be applied for different flow conditions, and eventually different wing geometries, a specific suction distribution may not achieve these basic goals. Therefore, the suction distribution investigated in this research has constant row spacing in the streamwise direction. However, the suction distributions designed based on Thwaites criterion of separation were used as the foundation for the average suction distribution used in this study. The average spacing between the suction rows was based on the results of the above analyses for the cases at $Re_c$ = 150,000 and 250,000 at $\alpha$ = 0, 2, 4 and 6 degrees.

The suction distribution consisted of suction rows in the streamwise direction extending between the two ends of the airfoil in the spanwise direction. The holes were distributed with 10 holes/inch (0.394 hole/mm) in the spanwise direction. The first row started at a location $x/c$ = 0.252 from the leading edge. The last row was located at $x/c$ = 0.495 with a distance of 1.5 mm (0.059 inch) between consecutive rows in the streamwise direction. This distance between the suction rows was on average 1.518 mm (0.06 inch) as a surface distance. The holes had a diameter of diameter 0.5 mm (0.02 inch).

Three suction distributions were investigated in this research and will be referred to as "Case 1", "Case 2" and "Case 3". In Case 1, suction was applied through the first 20 rows of holes. This distribution covered the distance from $x/c$ = 0.252 to 0.345. The suction distribution in Case 2 covered the distance between $x/c$ = 0.301 to 0.345, which better matches the results of the analysis obtained from the suction distribution design method explained above. The results suggest a starting point for the suction distribution at $x/c$ = 0.311 for the LA2573a airfoil at $Re_c$ = 250,000 at $\alpha$ = 2 degrees. However, an upstream starting point was chosen at $x/c$ = 0.301 to take into account the forward movement of the boundary layer separation point at higher angles of attack, at which drag measurements were carried out. The distribution labeled "Case 3" extended from $x/c$ = 0.252 to 0.495. Although the suction pump was not capable of providing enough differential pressure between the freestream and chamber pressures to ensure flow into the wing for this distribution, and although the application of the entire suction distribution was out of the scope of the study, its effects were investigated. The Case 3 investigation shows how the drag and boundary layer were affected by the presence of the holes without suction and with suction that was not sufficient to prevent separation. Table 1 summarizes the three suction distribution cases.

Table 1. Starting and Ending Locations of Suction Distributions Case 1, Case 2 and Case 3

| **Case** | **Starting *x/c*** | **Ending *x/c*** |
|---|---|---|
| 1 | 0.252 | 0.345 |
| 2 | 0.301 | 0.345 |
| 3 | 0.252 | 0.495 |

## III. Experimental Apparatus

The size and behavior of the LSB on a LA2573a airfoil was investigated at $Re_c$ = 250,000 and at different angles of attack. These results were documented (Wahidi and Bridges (2008)) and used as the basis for designing a suction distribution to control the size of the LSB. Another LA2573a airfoil model was constructed with a perforated upper surface and suction piping for testing the effectiveness of the designed suction distribution on controlling the size of the LSB and reducing the drag.

The experiments were conducted in the subsonic wind tunnel of the Department of Aerospace Engineering at Mississippi State University. This tunnel has an octagonal test section, measuring 1.463 m in length with a cross sectional area of 0.974 $m^2$. The maximum flow speed in the tunnel is 48.8 m/s and the freestream turbulence intensity is on average 0.58% for a speed range of 5-30 m/s.

Boundary layer measurements were carried out on the suction model at $Re_c$ = 250,000 at $\alpha$ = 2 degrees for Case 1, Case 2 and Case 3. In addition, boundary layer measurements were carried out at $Re_c$ = 250,000 and at $\alpha$ = 4 degrees for Case 2. Wake pressure measurements were carried out on the suction model at $Re_c$ = 250,000 and for $\alpha$ between -2 and 8 degrees to estimate the effects of applying suction on the drag.

The airfoil model had a chord length ($c$) of 0.3048 m and spanned the whole test section to create a nominally two-dimensional flow. The upper surface of this model was perforated using the CNC machine at the Center for Advanced Vehicular Systems (CAVS) at Mississippi State University. Although a multi-chamber suction configuration provides better control of the suction strength than a single-chamber configuration, only a single suction chamber was used in this research. The use of a single suction chamber provides simplicity in the design, construction and implementation necessary for unmanned aerial vehicles (UAVs).

Three stainless tubes with an inside diameter of 3.175 mm (0.125 inch) were placed in the suction chamber to measure the static pressure in the chamber to determine the pressure differential between the freestream and chamber static pressures.

A wake rake was constructed for the wake pressure measurements. The wake rake had 43 total pressure tubes with an inside diameter of 1.651 mm (0.065 inch) and 4 static pressure tubes with an inside

diameter of 3.175 mm (0.125 inch). Four holes with a diameter of 1.016 mm (0.04 inch) were drilled perpendicular to the flow on the static pressure tubes at 90 degrees intervals to measure the static pressure. The distance between the wake rake and the trailing edge of the airfoil was adjusted to one chord length (0.3048 m = 12 inches) by sliding the wake rake along its horizontal supports. The total and static pressure tubes were connected to a Pressure Systems, Inc., Model 9016 pressure scanner. The Model 9016 is a pneumatic intelligent pressure scanner with 16 integral pressure transducers, each with a full-scale range corresponding to 10 inches of water. The scanner has a measurement resolution of +/- 0.003% of the full scale. The coefficient of drag was estimated from the wake pressure measurements with an uncertainty of approximately 12%.

The freestream velocity is measured by a Pitot-static tube mounted at the entrance to the test section, with the total and static pressures being measured by the Model 9016 scanner. The uncertainty associated with the freestream velocity measurement is 0.8% leading to an uncertainty level of 0.85% in the Reynolds number calculation.

Measurements of the boundary layer mean and fluctuating velocities were carried out using a TSI Model 1750 constant-temperature hot-wire anemometer. The probe used for the velocity measurements was a TSI Model 1218-20 boundary-layer probe which was used to measure only the $u$ component of the flow. The hot-film probe has a platinum gas sensor with a diameter of 50.8 $\mu m$. Although a hot-wire has a better frequency response, a hot-film of this size was chosen because its larger size allows it to withstand measurements near the wall and the possibility of "touching" the wall while maintaining an adequate frequency response. Data were acquired at each measurement point at 2 kHz for a period of 5 seconds. The hot-film probe was tilted 25 degrees to provide space for the sensor to reach the surface of the airfoil in the convex region of the airfoil. A traversing system was mounted on top of the test section in order to traverse the hot-film probe in the longitudinal and vertical directions. The traversing system consisted of a vertical traverse and a longitudinal traverse. The vertical traverse was mounted on the longitudinal traverse and the probe was attached to the vertical traverse. The resolutions were 0.003175 mm and 0.1 mm for the vertical and longitudinal traverse systems, respectively. Each traverse in the boundary layer velocity profile measurements was conducted perpendicularly to the surface of the airfoil by traversing in both the vertical and the longitudinal directions.

The uncertainty associated with the mean velocity was on average 6% for attached laminar and turbulent boundary layer profiles. The uncertainty in the mean velocity was 8.2% and 16.1% for the separated and transitional velocity profiles, respectively. The absolute overall uncertainty associated with the displacement thickness ($\delta^*$) was 0.05 mm in the attached laminar and turbulent velocity profiles. The absolute overall uncertainty associated with the momentum thickness ($\theta$) was found to be 0.017 mm and 0.025 mm for the attached laminar and turbulent velocity profiles, respectively. The absolute uncertainty values in the momentum thickness measurements in the locations of separation and transition were estimated to be 0.015 mm and 0.013 mm, respectively. These values are not so much different than the uncertainty value in the attached laminar boundary layer. The absolute values of the uncertainty in the displacement thickness in the region of separated and transitional boundary layers were 0.082 mm and 0.1 mm, respectively.

The suction blower used to create vacuum inside the wing section was a Craftsman® portable blower model 17066. A "T"-connection with outlet diameters of 2 inches (0.051 m) was attached to the suction side of the blower, to which two hoses with an inside diameter of 1 inch (0.0254 m) were connected. The two hoses were connected to the two ends of the wing section in order to provide even suction from the wing. The suction strength was adjusted by varying the voltage supplied to the blower's motor. The volumetric flow rate was measured by a turbine flow meter Model 100 made by McMillan Company®. The measurement range for the flow meter was 100-500 liters per minute with an accuracy of $\pm$ 3.0% of full scale. This flow meter was connected to the discharge side of the blower.

## IV. Suction Results

### A. Experimental Procedure

As mentioned above, three cases, corresponding to three different suction distributions, were investigated for the LA2573a airfoil with suction. The measurements were carried out at $Re_c$ = 250,000.

The investigations in Case 1 consisted of drag and boundary layer measurements. The drag measurements were carried out at a range of $\alpha$ from -2 to 8 degrees for total suction rates (Q) of 100, 250 and 300 liters/minute. The boundary layer measurements were conducted at $\alpha$ = 2 degrees with a suction rate of 250 liters/minute, and consisted of measuring the boundary layer velocity profiles at different *x/c* locations. Drag measurements were conducted for Case 2 for the same range of angle of attack as in Case 1 at a suction rate of 250 liters/minute. Also, boundary layer measurements were carried out for Case 2 at $\alpha$ = 2 and 4 degrees. The drag measurements conducted for Case 3 were at the same conditions as in Case 1 and included the drag measurements with no suction applied. In addition, boundary layer measurements were conducted on the perforated airfoil with suction and without suction but with the holes uncovered in order to determine how the flow was modified by the presence of the holes.

The suction rate was set to a certain value before each set of experiments and the angle of attack was then changed. This procedure maintained a constant flow rate over the range of angles of attack except at the cases with a suction rate of 300 liters/minute. The reason for the slight changes in the suction flow rate at 300 liters/minute was due to the changes in the differential pressure between the edge and chamber pressures ($P_e$ - $P_c$) with a change in the angle of attack. At lower suction rates, the pump was capable of maintaining the pressure differential. However, at a suction rate of 300 liters/minute, the pressure differential requirements at higher angles of attack were more than the pump could produce. Figure 4 shows a plot of the $\Delta P_c$ normalized by the freestream dynamic pressure versus the suction coefficient for cases 1, 2 and 3 at different suction rates. The suction coefficient, $C_Q$, is defined as

$$C_Q = \frac{Q}{U_\infty cb} \tag{12}$$

where *b* is the span of the airfoil and *Q* is the flow rate, measured directly by a flow meter. The uncertainty in $C_Q$ ranged from 5.7 to 15.3%. The uncertainty bars are shown on one set of $C_Q$ values to give an indication of the uncertainty in the $C_Q$ values for a certain case.

The figure shows that the quantity $\Delta P_c/q$ increased vertically with increasing $\alpha$ for a given case at a given suction rate. The figure also shows that $\Delta P_c/q$ was much lower for Case 3 because the differential pressure applied was not sufficient to create an inflow over the region between *x/c* = 0.252 to 0.495. Some increase in $\Delta P_c/q$ was observed when the suction rate was increased from 100 to 250 liters/minute. However, no increase in $\Delta P_c/q$ was observed when the suction rate was increased from 250 to 300 liters/minute. It is clear in the figure that the suction distribution had a significant effect on $\Delta P_c/q$. This observation became clear when $\Delta P_c/q$ at a suction rate of 250 liters/minute was compared for the three cases. Case 2 had the shortest suction distribution and produced the highest differential pressure. These results and the drag results make it clear that to minimize the pumping requirements, that suction must be applied only over the region where it is required to prevent separation.

It is worth mentioning here that another definition of the suction coefficient ($C_{Q'}$) based on the actual length over which suction was applied could be investigated. Table 2 shows $C_Q$ and $C_{Q'}$ values corresponding to suction rates of 100, 250 and 300 liters/min for flow at $Re_c$ = 250,000 for the three suction distributions.

Table 2. $C_Q$ and $C_{Q'}$ Values for Different Suction Distributions at Different Suction Rates

| | $C_Q$ | $C_{Q'}$ |
|---|---|---|
| Case 1 – Q = 100 Liters/min | 3.75E-4 | 4.08E-3 |
| Case 1 – Q = 250 Liters/min | 9.37E-4 | 0.010 |
| Case 1 – Q = 300 Liters/min | 1.12E-3 | 0.012 |
| Case 2 – Q = 250 Liters/min | 9.37E-4 | 0.022 |
| Case 3 – Q = 100 Liters/min | 3.75E-4 | 1.54E-3 |
| Case 3 – Q = 250 Liters/min | 9.37E-4 | 3.86E-3 |
| Case 3 – Q = 300 Liters/min | 1.12E-3 | 4.63E-3 |

**B. Boundary Layer Results**

Because no surface pressure distributions could be obtained on the model with suction, detailed boundary layer measurements were required. The boundary layer measurements conditions were fixed based on the most promising drag reduction results as will be discussed in Section IV.C. These conditions were at a suction rate of 250 liter/min and $\alpha$ = 2 degrees for Case 1, 2 and 3. In addition, boundary layer measurements were carried out at a suction rate of 250 liter/min and $\alpha$ = 4 degrees for Case 2. Figures 5 and 6 compare the mean and fluctuating velocity profiles, respectively, for the solid model and for the suction distribution of Case 1 with a suction rate of 250 liters/minute. It is seen in the figures that applying suction with this distribution maintained an attached flow until the transition point (identified as the location where the separated shear layer on the solid airfoil transitions from laminar to turbulent at $x/c$ = 0.372). The baseline mean velocity profile at $x/c$ = 0.315 represented the separation location. The corresponding fluctuating velocity profile shows a slight increase when compared to the same profiles in the laminar region. The mean and fluctuating velocity profiles of Case 1 at this location appeared to be attached and no sign of an inflection point was observed in the mean velocity profile. The transition location of the baseline case was at $x/c$ = 0.372. The boundary layer remained attached at this location when suction was applied and the transition occurred at $x/c$ = 0.401 as can be seen in Figs. 5 and 6. The mean velocity profile of the case with suction did not indicate any separation of the laminar boundary layer at $x/c$ = 0.372; however, the fluctuating velocity exhibits a slight increase at this location. This increase is relatively of the same magnitude as of the increase in the fluctuating velocity for the baseline at the separation location at $x/c$ = 0.315. These observations indicate that the boundary layer remained attached until shortly downstream of terminating the suction at $x/c$ = 0.345. The boundary layer then separated and transitioned at a downstream location relative to the baseline location (*i.e.* at $x/c$ = 0.401). Therefore, the application of suction was capable of delaying separation and transition. A possible reason for the apparent attached flow at $x/c$ = 0.372 is that with the suction applied, the reversed flow region could have been very small and close to the airfoil surface which would have made it difficult to be distinguished with the hot-film measurement. This reasoning is further supported by observing the fluctuating velocity profiles at $x/c$ = 0.401, 0.43 and 0.46. It is observed in these profiles that the heights of the increase in the fluctuating velocities are much less than the heights observed in the baseline fluctuating velocity profiles at $x/c$ = 0.315, 0.372 and 0.43. A comparison of the transitional mean velocity profiles of the two cases, i.e. $x/c$ = 0.372 and 0.401, shows that the height of the reversed flow region was much less when suction was applied. Therefore, applying suction significantly decreased the length of the laminar portion of the bubble and its height. The suction distribution of Case 1 ended at $x/c$ = 0.345. This location was upstream of the baseline transition location at $x/c$ = 0.372. Suppose that it was desired to maintain the transition location at its baseline location (*i.e.* $x/c$ = 0.372). Because of the "gap" between the end of suction and transition, the termination of suction would have to be upstream of $x/c$ = 0.345, resulting in a shorter suction region. Applying suction over a shorter distance permits more concentrated suction and correspondingly higher suction velocities. Therefore, a greater decrease in drag could be achieved for the same suction rate. This will be seen in the next section in a comparison of the drag reduction results between Cases 1 and 2 at a suction rate of 250 liters/minute. For Case 1, the boundary layer appeared to reattach at the same location at $x/c$ = 0.52 where typical turbulent boundary layer profiles were observed. The suction did not appear to affect the development of the boundary layer downstream of reattachment for this case as can be seen by the identical velocity profiles in the turbulent boundary layer region. Since the separation was delayed and the reattachment location of the separated boundary layer remained unchanged, it was concluded that total length of the LSB decreased by applying suction using the distribution of Case 1. Also, it was found that the turbulent portion of the LSB decreased in length while the length of the laminar portion did not change.

Figures 7 and 8 show the mean and fluctuating velocity profiles measurements carried out for Case 2 suction distribution with a suction rate of 250 liters/minute at $Re_c$ = 250,000 at $\alpha$ = 2 degrees. The velocity profiles in some locations do not start from the airfoil surface because some of the near-wall measurements were unreliable due to the heat transfer effects between the hot film and the airfoil surface. Figure 7 shows that the laminar boundary layer remains attached until $x/c$ = 0.372. This is also confirmed by the low fluctuations in the velocity profiles as shown in Fig. 8. The fluctuating velocity profiles of the baseline results show a slight increase in the fluctuation level at the separation location at $x/c$ = 0.315. When suction was applied in the Case 2 distribution, the mean velocity profile at $x/c$ = 0.401 shows a slight deviation from the attached laminar velocity profiles upstream as an indication of separation. The fluctuating velocity profile at this location shows an increase in the level of turbulence. However, this increase has a much

smaller magnitude in comparison to the equivalent increase of the baseline result at $x/c$ = 0.315. The location of transition is determined by the apparent reversed flow region in the mean velocity profiles and the appearance of large turbulence level in the fluctuating velocity profiles. This behavior can be clearly seen at $x/c$ = 0.46 for Case 2 suction distribution. However, the height of the reversed region is much smaller when suction was applied as compared to the baseline results at $x/c$ = 0.372. The reattachment location for Case 2 distribution at $\alpha$ = 2 degrees was determined at $x/c$ = 0.579 based on the fully turbulent boundary layer velocity profiles as seen in Fig. 7. The above results show that applying suction at the distribution of Case 2 at $\alpha$ = 2 degrees with a rate of 250 liter/min caused a separation delay from $x/c$ = 0.315 to 0.401, a transition delay from $x/c$ = 0.372 to 0.46 and a reattachment delay from $x/c$ = 0.52 to 0.579. Therefore, the total length of the LSB decreased. However, the laminar portion of the bubble remained approximately constant and the turbulent portion of the bubble decreased. The total length of the bubble and the lengths of the laminar and turbulent portions of bubble are approximately the same as those obtained by applying the same suction rate at the suction distribution of Case 1 as presented above in Figs 5 and 6.

The mean and fluctuating velocity profiles for the suction distribution of Case 2 with a suction rate of 250 liter/min at $\alpha$ = 4 degrees are compared with those of the baseline results in Figs. 9 and 10, respectively. The boundary layer separates at $x/c$ = 0.343 when suction was applied while the boundary layer separates at $x/c$ = 0.315 for the baseline results. This is observed by the slight increase in the turbulence level and the small reversed flow region at this location. The mean velocity profiles in Fig. 9 do not show a larger reversed flow region as an indication of the transition location. However, an inspection of the fluctuating velocity profiles in Fig. 10 shows a larger turbulence level at $x/c$ = 0.43, which can be assumed as the transition location. The mean velocity profiles show that the reattachment location was at $x/c$ = 0.49. However, the turbulent velocity profiles for this case study do not fully coincide with the turbulent velocity profiles of the baseline results until $x/c$ = 0.748. This could be an indication that suction affected the development of the turbulent boundary layer far downstream of the reattachment location. This observation is also supported by investigating the fluctuating velocity profiles shown in Fig. 10. It is seen in the figure that the turbulence level in the turbulent boundary layer region, i.e. 0.49 > $x/c$ > 0.666, is less than that in the baseline results.

Figures 11 and 12 compare the mean and fluctuating velocity profiles, respectively, of Case 2 at $\alpha$ = 2 and 4 degrees. It can be seen in the figures that the mean and fluctuating turbulent velocity profiles at $x/c$ = 0.666 and 0.748 are identical. Therefore, the effect of suction on the development of the turbulent boundary layer becomes similar far downstream of the reattachment location.

Boundary layer measurements were carried out for the Case 3 suction distribution without suction and with a suction rate of 250 liters/minute at $Re_c$ = 250,000 at $\alpha$ = 2 degrees. The mean and fluctuating velocity profiles of these measurements are shown in Figs. 13 and 14. The suction distribution of Case 3 covered the distance from $x/c$ = 0.252 to 0.495. It is seen in the Fig. 14 that this distribution caused an earlier transition at $x/c$ = 0.286 as compared to 0.372 for the baseline case. This is observed by the first appearance of an increase in the turbulence level. The location of transition at this distribution did not change with or without suction. This result was expected since the suction rate at this suction distribution was not sufficient to cause an inflow over the entire perforated region. The edge pressure distribution showed that the required $\Delta P_c$ should have been 96.5 Pa in order to achieve inflow over the entire perforated region of Case 3; however, $\Delta P_c$ at this condition was only 36.4 Pa. Therefore, it is probable that there was outflow over some portions of the perforated region. The earlier transition was probably due to the presence of outflow in the region of lower edge pressure. The velocity profiles in the turbulent region showed a deviation when suction was applied. It can also be seen in the figure that this deviation increased with increasing $x/c$ in a region characterized by higher edge pressure. This deviation was mainly due to the larger differential pressure between the edge pressure and the chamber pressure which allowed for the suction to be more effective in that region. Applying suction did not affect the turbulence level in the boundary layer as can be seen in Fig. 14.

Figure 15 compares the distributions of the displacement thicknesses of Case 1, Case 2 at $\alpha$ = 2 and 4 degrees and those of the baseline at $\alpha$ = 2 and 4 degrees. The displacement thickness ($\delta^*$) of the baseline suddenly grows after the separation point. The increased rate of growth of the displacement thickness after separation can be used to estimate the location of separation. This increasing rate of growth corresponds to the increasing thickness of the reversed flow region. This growth continues at approximately similar rate until a maximum is reached downstream of the transition location. The displacement thickness slightly

decreases downstream of the transition location and then grows gradually. This typical behavior is clearly seen in the figure for baseline results and in an agreement with previous studies, such as Albano *et al*. (2006), LeBlanc (1992), Mangalam *et al*. (1985) and Fitzgerald and Mueller (1990). The distributions for Case 1, and Case 2 at $\alpha$ = 2 and 4 degrees did not behave in the typical fashion as they did not exhibit a peak at the transition location. The values of $\delta^*$ for Case 1 were, in general, higher than those of Case 2 and baseline results. The displacement thickness for Case 1 distribution suddenly increased after $x/c$ = 0.372. The transition location for this was found to be at $x/c$ = 0.401 from the analysis of the boundary layer velocity profiles. The displacement thickness continued to grow downstream of $x/c$ = 0.401 at a higher rate than its growth in the laminar region. Similar behavior was observed in the distribution of $\delta^*$ for Case 2 at $\alpha$ = 2 degrees. It can be seen in the figure that the growth rate of $\delta^*$ downstream of the transition location of Case 1 at $x/c$ = 0.401 is comparable with that of Case 2 at $\alpha$ = 2 degrees downstream of separation at $x/c$ = 0.401. The behavior of $\delta^*$ was different for Case 2 at $\alpha$ = 4 degrees than that for the same case at $\alpha$ = 2 degrees. In this case $\delta^*$ increases at a relatively constant rate with no sudden increase at the separation or transition locations.

The distributions of the momentum thickness ($\theta$) for the same cases in Fig. 15 are shown in Fig. 16. It is seen in the figure that the rate of growth of $\theta$ of all the cases significantly increases at the transition location, and, $\theta$ continues to grow. The rate of growth of $\theta$ appeared to be similar in all the cases. It is deduced from the behavior of $\theta$ of the baseline results that the growing thickness of the reversed flow region has only a small effect on the growth of the momentum thickness since no significant change was observed between the locations of separation and transition. Therefore, it was not expected to observe this small effect in Case 1 and Case 2 as the height of reversed flow region was very small. Comparison between the distributions of the $\theta$ of Case 1 and Case 2 at $\alpha$ = 2 and 4 degrees shows that the more concentrated suction obtained by Case 2 distribution causes a reduction in the values of $\theta$.

The distributions of the shape factor ($H$) for the cases in Fig. 15 are shown in Fig. 17. The shape factor of a flow with an LSB increases after the separation location and then continues to gradually increase to reach a maximum value at transition, after which it gradually decreases to lower values in the turbulent region as was seen in the results of LeBlanc (1992). The shape factor of the baseline results shows an abrupt increase after separation and reaches a maximum value at transition due to the increase in the displacement thickness. Similar to the displacement thickness, the shape factor can also be investigated to locate the point of separation based on the obvious sudden increase after separation. The peak in the shape factor is a good indication of the existence of the laminar separation bubble since a flow that undergoes transition without separation would show a gradual decrease in the shape factor from the values for attached laminar flow to the lower value corresponding to the turbulent boundary layer. Investigation of the mean and fluctuating velocity profiles shows that the location of the peak in $H$ corresponds to the location of transition. The values of $H$ are identical for all the cases downstream of the reattachment location, reaching a nominal value of 1.37 which is typical of a fully turbulent boundary layer. These lower shape factor values observed in all the cases can also be a way to define the location of reattachment. Since the points of separation, transition and reattachment are well defined in the plot of the shape factor, it can be used to define the size and the location of the separation bubble, without having to resort to surface pressure measurements. This observation was of great importance for this research since it allowed for the construction of wing sections for investigating the effects of distributed suction that did not require the ability to measure the surface pressures. The shape factor distributions of Case 1 and Case 2 at $\alpha$ = 2 degrees exhibited the expected peak at the transition location. However, the value of the shape factor of Case 1 suddenly increased from the laminar values to its peak at the transition location. The sudden increase of the shape factor of Case 1 from the laminar values to the maximum values at transition indicated that applying suction caused the reversed flow region to be very small to affect the distribution of the shape factor. These observation provided confidence in using suction to control the size and location of the laminar separation bubble. Also, the results showed the effectiveness and the applicability of the suction distribution design method based on Thwaites' criterion at separation. It was observed from the mean and fluctuating velocity profiles that the boundary layer of Case 3 with and without suction transitioned upstream of the baseline transition location. Therefore, it can be concluded that the LSB was eliminated. However, the presence of the peak in the shape factor, not shown here, at the transition location of Case 3 remaines unexplained and requires further investigation.

Figure 18 summarizes the above results of the locations of separation (S), transition (T) and reattachment (R) for the baseline results and those obtained by investigating the suction distributions of Case 1 and Case 2 at a suction rate of 250 liter/minute.

**C. Drag Results**

Figure 19 compares the baseline and Case 1 $C_d$ results. The drag results for the perforated airfoil with the Case 1 hole distribution but without suction are also included in the figure. The $C_d$ values of Case 1 without suction are higher than the baseline results. The reason for the higher drag could be due to the outflow from the suction holes which could cause an earlier transition which increases the skin friction drag. An application of a suction rate of 100 liters/minute ($C_{Q'}$ = 4.08E-3) decreased $C_d$ values to the baseline values. However, increasing the suction rate to 250 liters/minute ($C_{Q'}$ = 0.01) decreased the drag below the baseline drag by an average value of 14%. A further increase in the suction rate to 300 liters/minute ($C_{Q'}$ = 0.012) resulted in an average decrease of drag of 24% below the baseline drag. The decrease in $C_d$ is beyond the uncertainty of $C_d$ for the solid airfoil. The decrease in drag between the cases with suction rates of 250 and 300 liters/minute ($C_{Q'}$ = 0.01 and 0.012) is within the uncertainty of the results of Case 1 with a suction rate of 250 liters/minute ($C_{Q'}$ = 0.01). However, all drag results were compared with the drag values of the solid airfoil. Also, the drag reduction was not only seen at a certain angle of attack but on all the angles of attack investigated. Therefore, it is reasonable to conclude that increasing the suction rate from 250 to 300 liters/minute ($C_{Q'}$ = 0.01 to 0.012) caused a further reduction in drag.

The comparison of the $C_d$ results for Case 2 at a suction rate of 250 liters/minute ($C_{Q'}$ = 0.022), baseline and Case 1 at suction rates of 250 and 300 liters/minute ($C_{Q'}$ = 0.01 and 0.012) is shown in Fig. 20. It is seen in the figure that the suction distribution in Case 2 required only 250 liters/minute ($C_{Q'}$ = 0.022) to show a decrease in drag greater than the decrease obtained with 300 liters/minute ($C_{Q'}$ = 0.012) applied at the suction distribution of Case 1. This was mainly due to the more-concentrated suction which was believed to have a stronger effect on modifying the inflection point of the separating velocity profiles. Also, the suction distribution for Case 2 was applied slightly upstream of the location of $\lambda = \lambda_0$ as determined from the analysis above whereas it was applied much upstream of $\lambda = \lambda_0$ in Case 1 and Case 3. This result is consistent with the applicability of the suction distribution method discussed in this work where the suction becomes more effective if it is applied shortly before the location of separation defined as $\lambda_0 = -0.09$.

Figure 21 presents the drag results obtained from Case 3 with and without suction. The suction distribution of Case 3 resulted in 20% higher drag when no suction was applied. Applying suction at a rate of 100 liters/minute ($C_{Q'}$ = 1.54E-3) reduced the drag by 5%, but the drag was still higher than the baseline drag. Increasing the suction rate to 250 and 300 liters/minute ($C_Q$ = 3.86E-3 and 4.63E-3) caused a reduction in drag to about the baseline drag values. A reduction in drag was not expected with the suction distribution of Case 3; however, the results of this case are important since they demonstrated the negative effects of not applying enough suction.

This observation has to be taken into account when a suction distribution is applied to a vehicle operating in the low Reynolds number regime. A suction distribution that is designed for certain flight conditions could result in severe negative effects at off-design conditions. Therefore, the suction pump has to be oversized to provide enough suction to counteract the negative effects at off-design conditions.

**C. Cost of Suction**

Carmichael (1954a; see also Bridges (2006)) introduced a method to compute the cost of suction. His idea was based on determining the required power to raise the chamber static pressure to the freestream static pressure such that

$$P_{suction} = (P_\infty - P_c)Q = \Delta PQ \tag{13}$$

where $Q$ is the total suction volumetric flow rate and $\Delta P$ is the difference between the freestream and chamber static pressures. This is an "ideal" power in that it neglects losses in ducting and other components that would be present in an actual mechanical suction system. The power associated with the equivalent suction drag $D_s$ was set to $P_{suction}$, such that

$$P_{suction} = D_s U_\infty = \Delta PQ \tag{14}$$

Solving for $D_s$ from Eq. (14) gives,

$$D_s = \frac{\Delta P Q}{U_\infty} \tag{15}$$

By using Eq. (15), the coefficient of equivalent suction drag can be written as

$$Cd_s = \frac{D_s}{q_\infty S_{ref}} = \frac{\Delta P}{q_\infty} \frac{Q}{U_\infty S_{ref}} = \frac{\Delta P}{q_\infty} C_Q \tag{16}$$

The net drag was computed as:

$$Cd_{net} = Cd_{suction} + Cd_s \tag{17}$$

In order to assess the advantage of applying suction to reduce the drag, the cost of suction must be taken into account. This assessment was accomplished by computing the decrease in the drag coefficient obtained by applying suction and then dividing this decrease in drag by the suction drag coefficient.

A figure of merit (FOM) quantifies the gain, if any, from applying suction. It is introduced in Eq. (18)

$$FOM = \frac{Cd_{baseline} - Cd_{suction}}{Cd_s} \tag{18}$$

The figure of merit was computed for the cases where there was a reduction in drag. This was seen in Case 1 with a suction rate of 250 and 300 liters/min ($C_{Q'}$ = 0.01 and 0.012) and in Case 2 with a suction of 250 liter/min ($C_{Q'}$ = 0.022). A figure of merit of more than one indicates that the gain in reducing the drag by using suction is more than the cost associated with using suction.

The values of the FOM at different $\alpha$ were averaged over the range of angles of attack. The average value of FOM for Case 1 with a suction rate of 250 liters/minute ($C_{Q'}$ = 0.01) was 3.8. The average decrease in drag for this case was 14%. Increasing the suction rate from 250 to 300 liters/minute ($C_Q$ = 0.01 to 0.012) caused an increase in FOM to 4.1 and an average reduction in drag of 24%. The average FOM value for Case 2 was 4.1 for an average decrease in drag of 24%. Therefore, concentrating the suction distribution between a point shortly upstream of separation to a point just upstream of transition provides better control of the size of LSB, and a greater decrease in drag for the same suction rate. In other words, a greater reduction in drag can be achieved for the same suction rate if the suction is applied at the right location.

Figure 22 shows the values of FOM with $\alpha$ for Case 1 with 250 and 300 liters/minute suction rates ($C_{Q'}$ = 0.01 and 0.012), and Case 2 with a suction rate of 250 liters/minute ($C_{Q'}$ = 0.022).

## IV. Conclusions

The results showed that the suction distribution designed in this work was effective in controlling the size of the laminar separation bubble, delaying separation, and controlling the location of transition. The effects of different suction rates and distributions on the drag were investigated. Drag reductions of 14-24% were achieved. A figure of merit defined as drag reductions divided by the equivalent suction drag was used to assess the worthiness of the utilizing suction on low Reynolds number flows. The values of the figure of merit were around 4.0 which proved that the penalty of using suction was significantly less than the gain obtained in reducing the drag.

### References


[1] Albano, F., Auletta, A. and De Gregorio, F., 2006, "An Experimental Study of Laminar Separation Bubbles on Airfoil at Low Reynolds," *AIAA Paper No. 2006-3529, presented at the 36th AIAA Flow Dynamics Conference and Exhibit, 5-8 June 2006, San Francisco, California.*

[2] Bridges, D. H., 2007, "Early Flight Test and Other Boundary Layer Research at Mississippi State 1949-1960," *J. Aircraft, **44** (5), September – October 2007, pp. 1635-1652.*

[3] Carmichael, B. H., 1954, "Suction Stabilized Boundary Layers," *Aeronautical Engineering Review, **13** (2),* February 1954, *pp. 36-41*.

[4] Crabtree, L. F., 1959 "The Formation of Regions of Separated Flow on Wing Surfaces," ARC R& M No. 3122, 1959.

[5] Fitzgerald, E. J., and Mueller, T. J., 1990, "Measurements in a Separation Bubble on an Airfoil Using Laser Velocimetry," *AIAA Journal*, ***28*** *(4), pp. 584–592.*

[6] LeBlanc, P. J., 1992 "An Experimental Investigation of Transitional Instabilities in Laminar Separation Bubble Flows on Airfoils Operating at Low Reynolds Numbers," PhD Dissertation, University of Southern California.

[7] Mangalam, S., Meyers, J., Dagenhart, J. and Harvey, W., 1985 "A Study of Laminar Separation Bubble in the Concave Region of an Airfoil using Laser Velocimetry," *Symposium on Laser Anemometry, ASME 1985 Winter Annual Meeting, 17-21 November 1985, Miami, Florida*.

[8] Wahidi, R., and Bridges, D. H. 2008 Control of Laminar Separation Bubbles with Distributed Suction – Preliminary Studies. *AIAA Paper No. 2008-738, presented at the 46th AIAA Aerospace Sciences Meeting, 7-10 January 2008, Reno, Nevada.*

[9] Wahidi, R., and Bridges, D. H. 2009 Experimental Investigation of the Boundary Layer and Pressure Measurements on Airfoils with Laminar Separation Bubbles. *AIAA Paper No. 2009-4278, presented at the 39th AIAA Fluid Dynamics Conference, 22-25 June 2009, San Antonio, Texas.*

[10] White, F. M., 2005, *Viscous Fluid Flow*, 3rd edition, McGraw-Hill, New York.

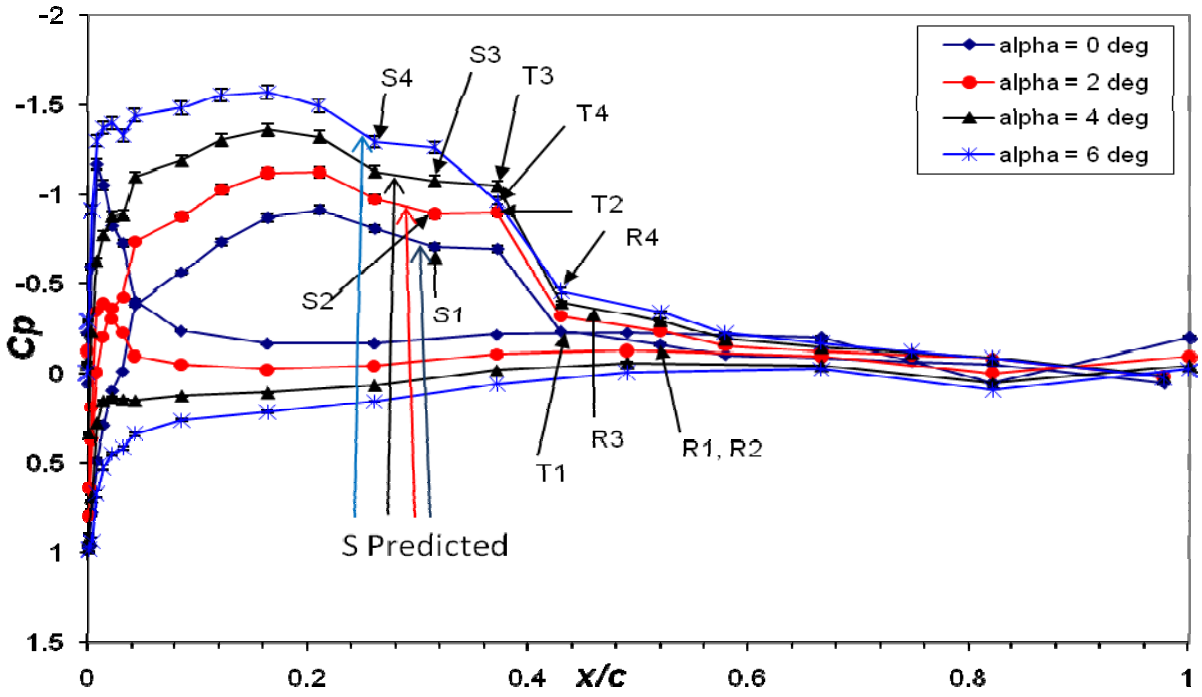


**Figure 1 *Cp* on LA2573a at $Re_c$ = 250,000**

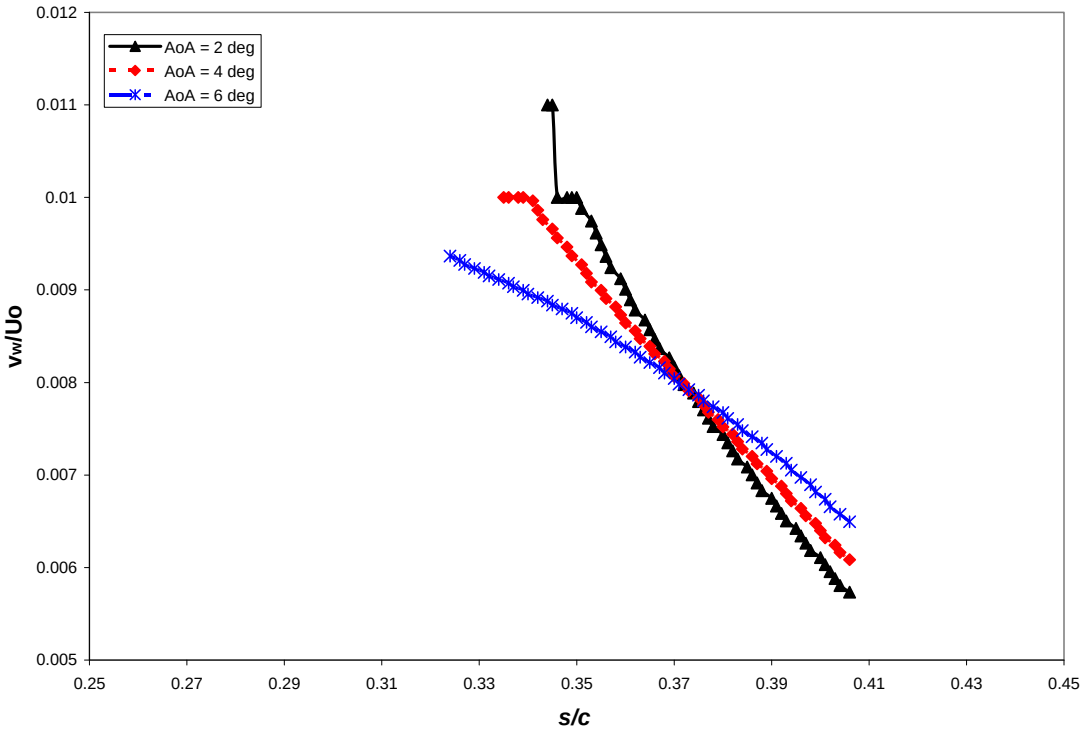


**Figure 2 Predicted Suction Velocity Distributions for LA2573a at $Re_c$ = 250,000 at $\lambda_0$ = -0.08**

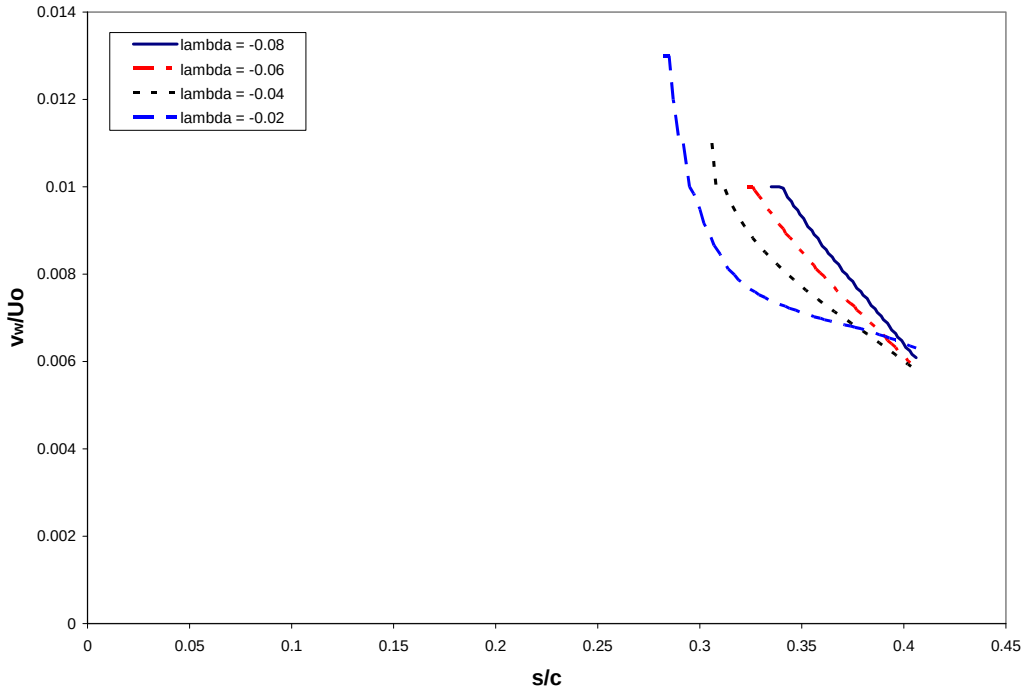


**Figure 3 Predicted Suction Velocity Distributions for LA2573a at α = 4 Degrees for Different Values of $\lambda_0$**

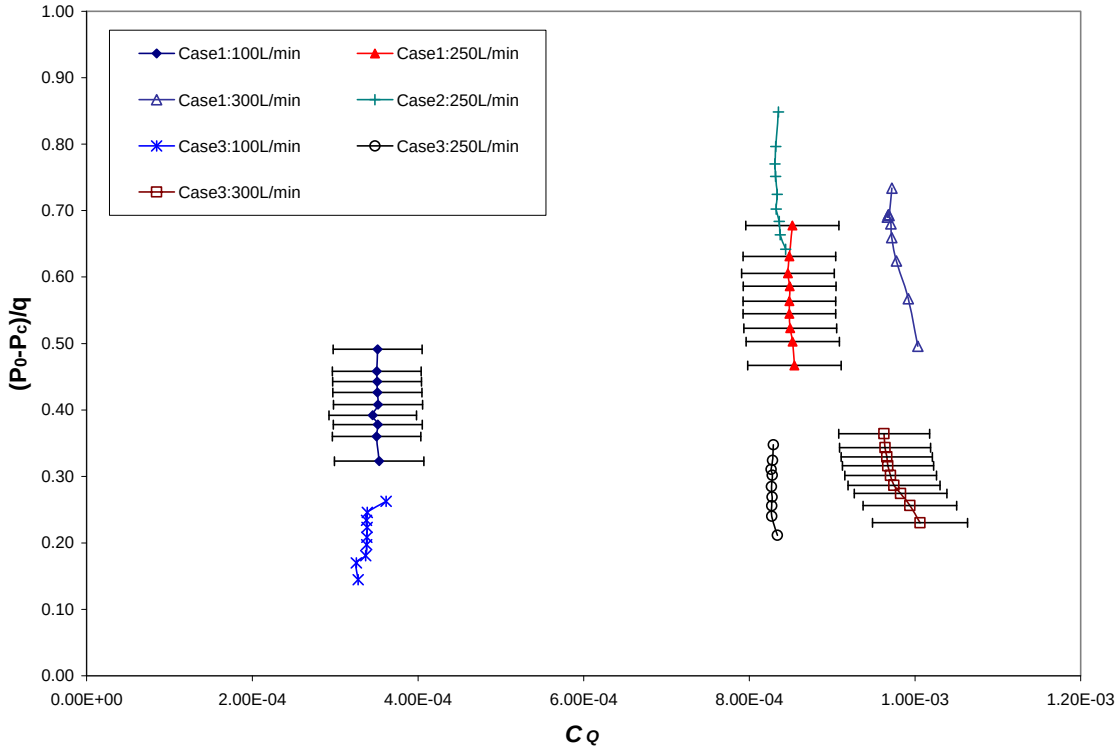


**Figure 4 A Plot of $\Delta P_c/q$ versus $C_Q$ for Case 1, 2 and 3 at Different Suction Rates**

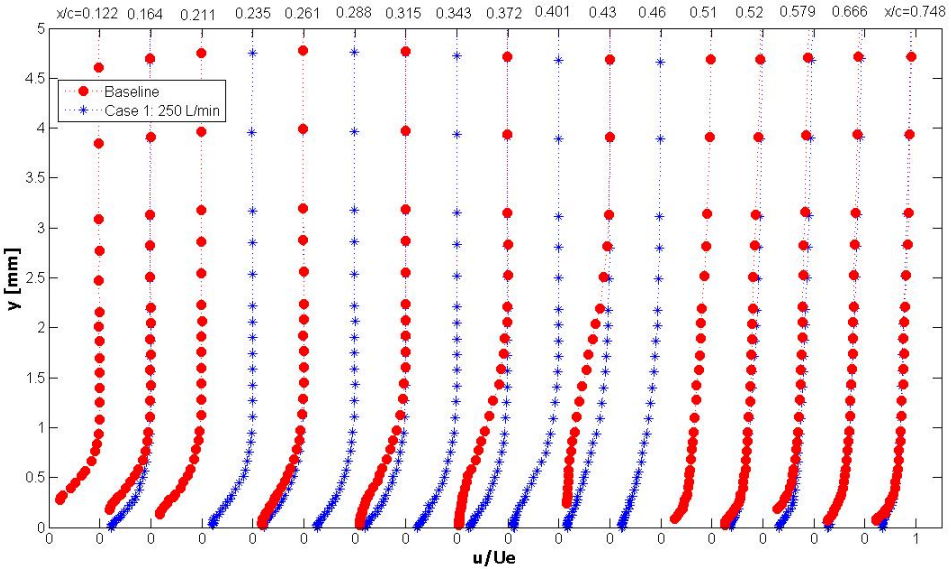


**Figure 5. Comparison between Baseline and Case 1 Mean Velocity Profiles (Suction for 0.252 < *x/c* < 0.345)**

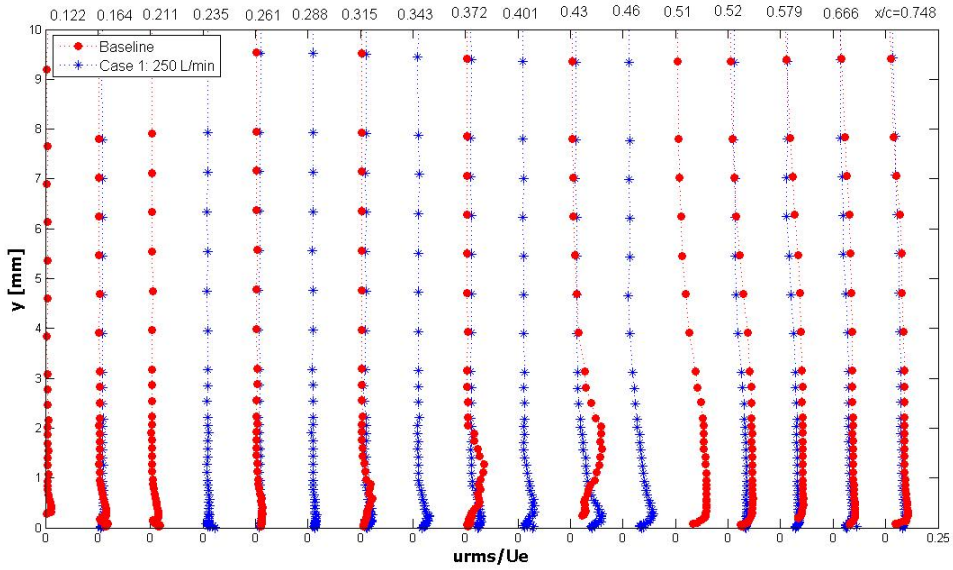


**Figure 6. Comparison between Baseline and Case 1 Fluctuating Velocity Profiles (Suction for 0.252 < *x/c* < 0.345)**

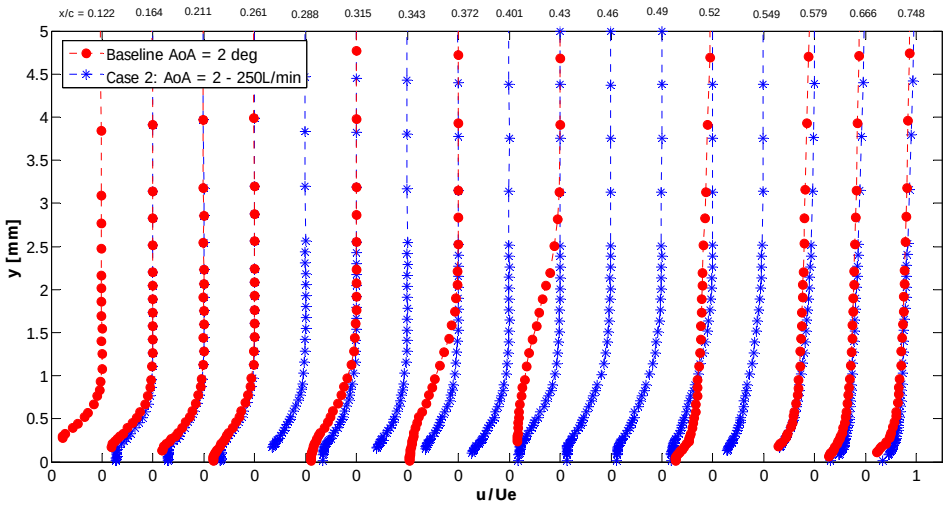


**Figure 7. Comparison between Mean Velocity Profiles of Baseline and Case 2 at α = 2 degrees (Suction for 0.301 < *x/c* < 0.345)**

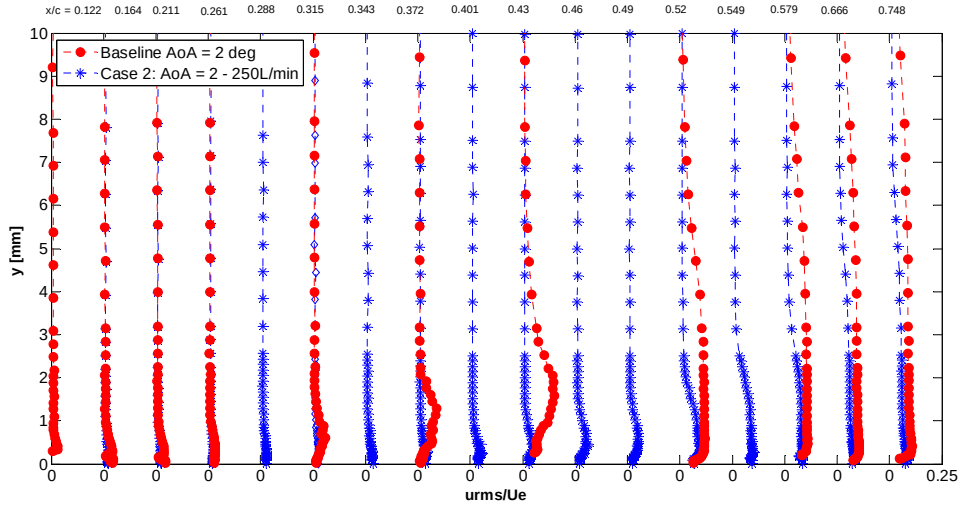


**Figure 8. Comparison between Fluctuating Velocity Profiles of Baseline and Case 2 at α = 2 degrees (Suction for 0.301 < *x/c* < 0.345)**

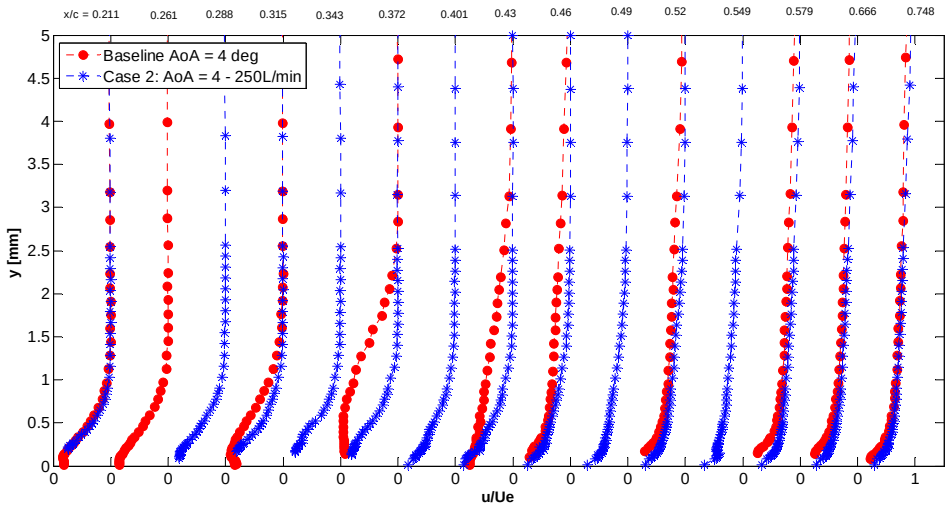


**Figure 9. Comparison between Mean Velocity Profiles of Baseline and Case 2 at α = 4 degrees (Suction for 0.301 < *x/c* < 0.345)**

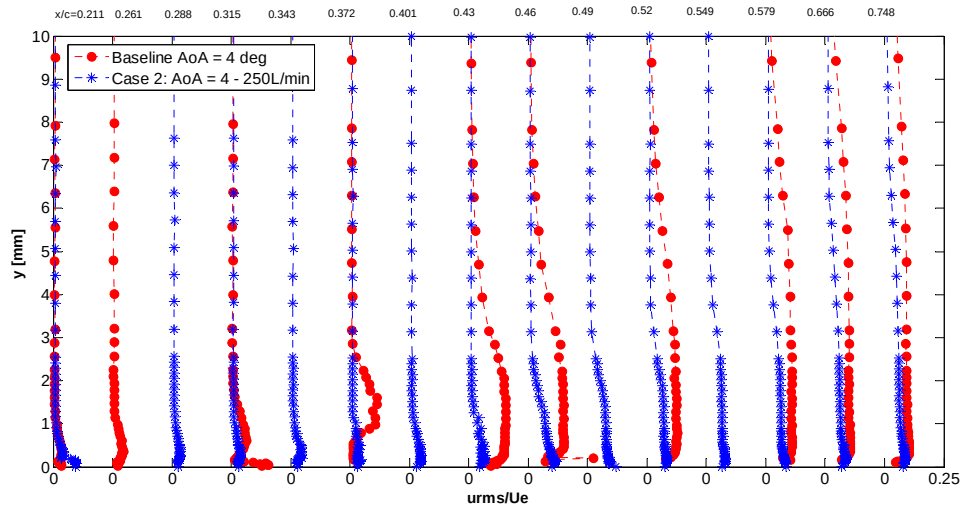


**Figure 10. Comparison between Fluctuating Velocity Profiles of Baseline and Case 2 at α = 4 degrees (Suction for 0.301 < *x/c* < 0.345)**

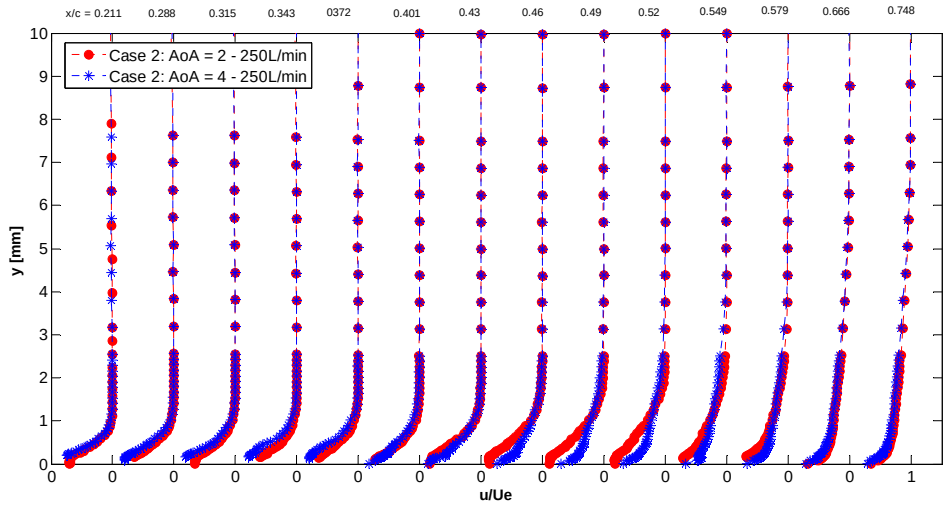


**Figure 11. Comparison between Mean Velocity Profiles of Case 2 at α = 2 and 4 degrees (Suction for 0.301 < *x/c* < 0.345)**

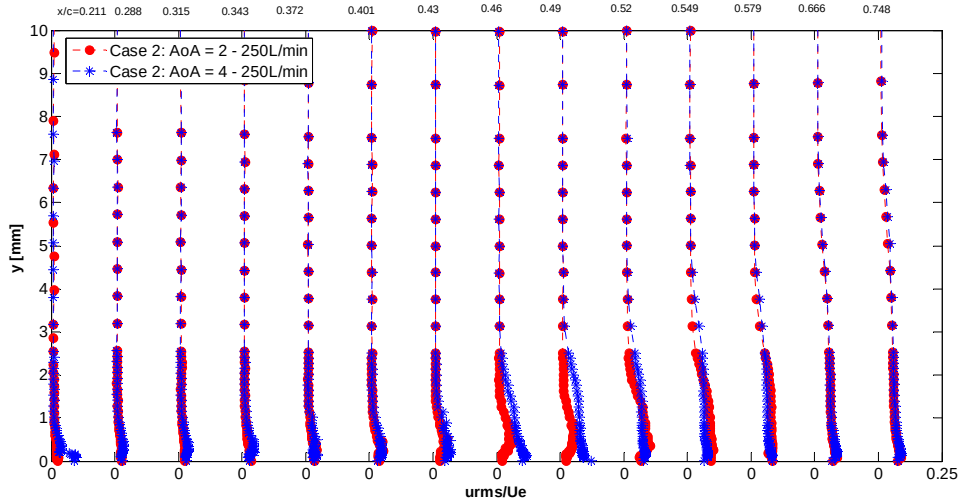


**Figure 12. Comparison between Fluctuating Velocity Profiles of Case 2 at α = 2 and 4 degrees (Suction for 0.301 < *x/c* < 0.345)**

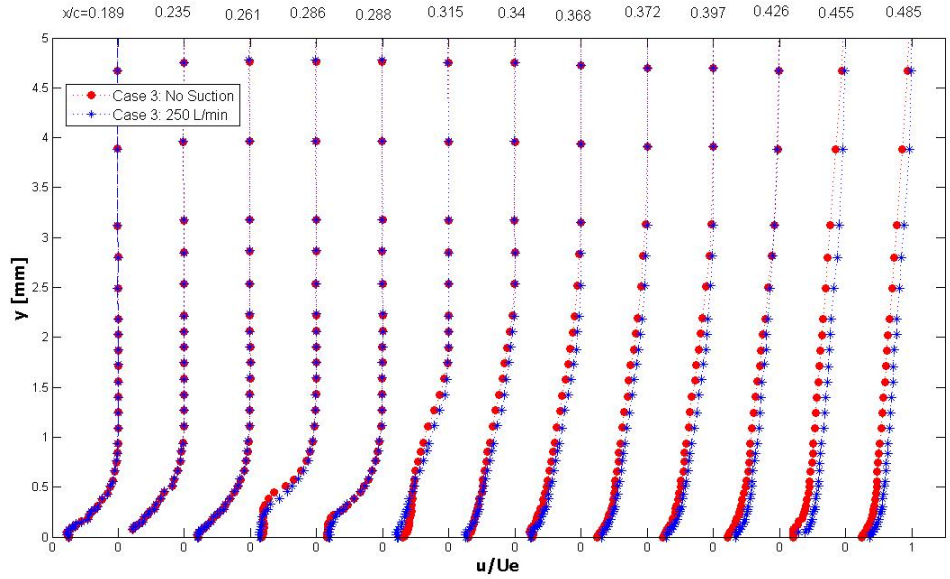


**Figure 13 Comparison between Case 3 Mean Velocity Profiles with and without Suction (Suction for 0.252 < *x/c* < 0.495)**

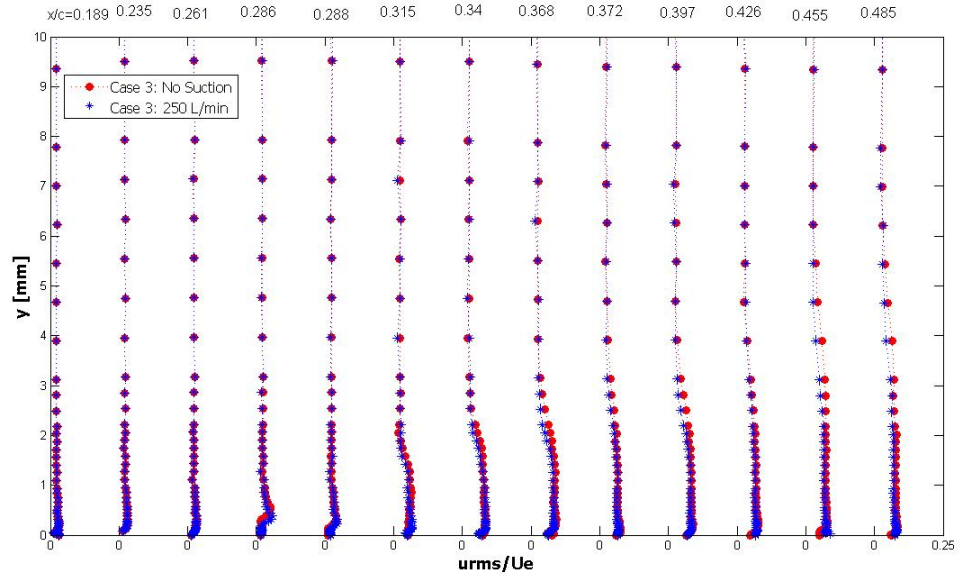


**Figure 14 Comparison between Case 3 Fluctuating Velocity Profiles with and without Suction (Suction for 0.252 < *x/c* < 0.495)**

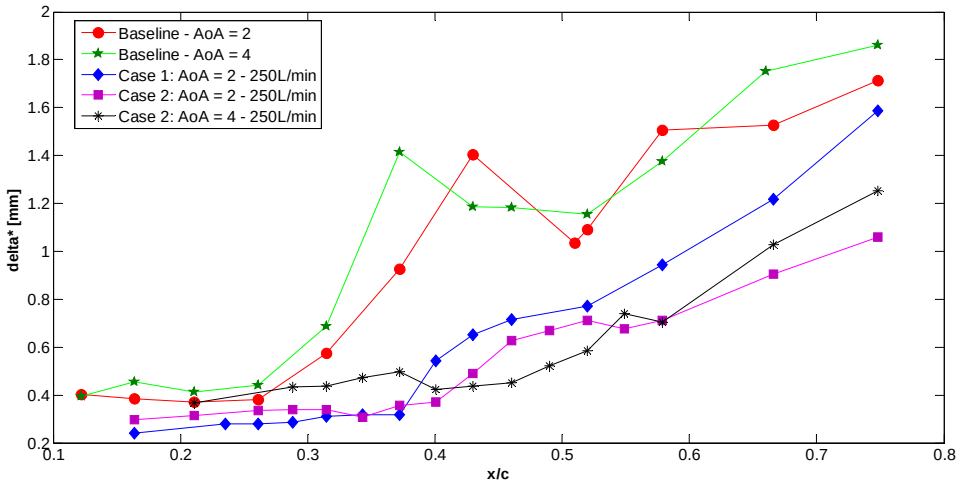


**Figure 15 Distribution of Displacement Thickness for Case 1 and Case 2**

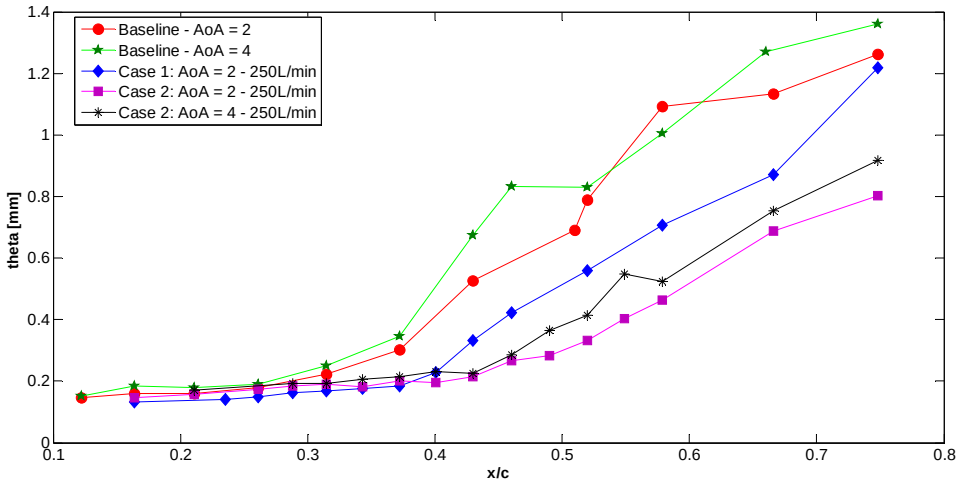


**Figure 16 Distribution of Momentum Thickness for Case 1 and Case 2**

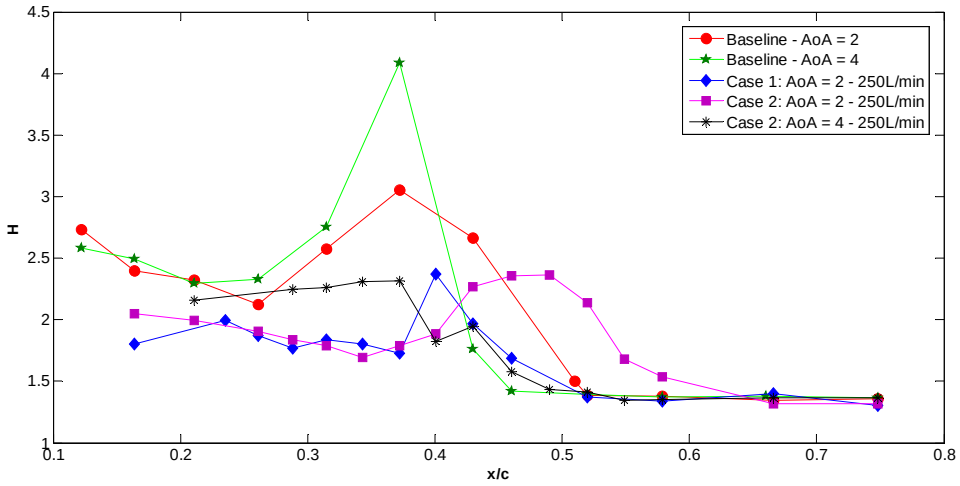


**Figure 17 Distribution of Shape Factor for Case 1 and Case 2**

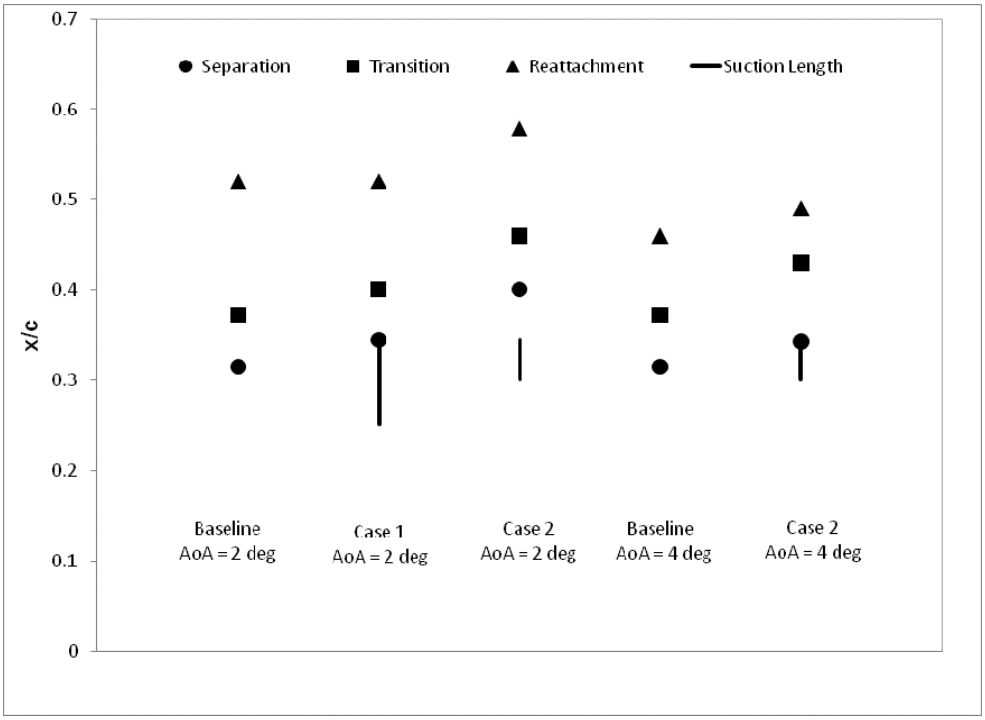


**Figure 18 Summary of Different Suction Distributions and Locations of Separation (S), Transition (T) and Reattachment (R)**

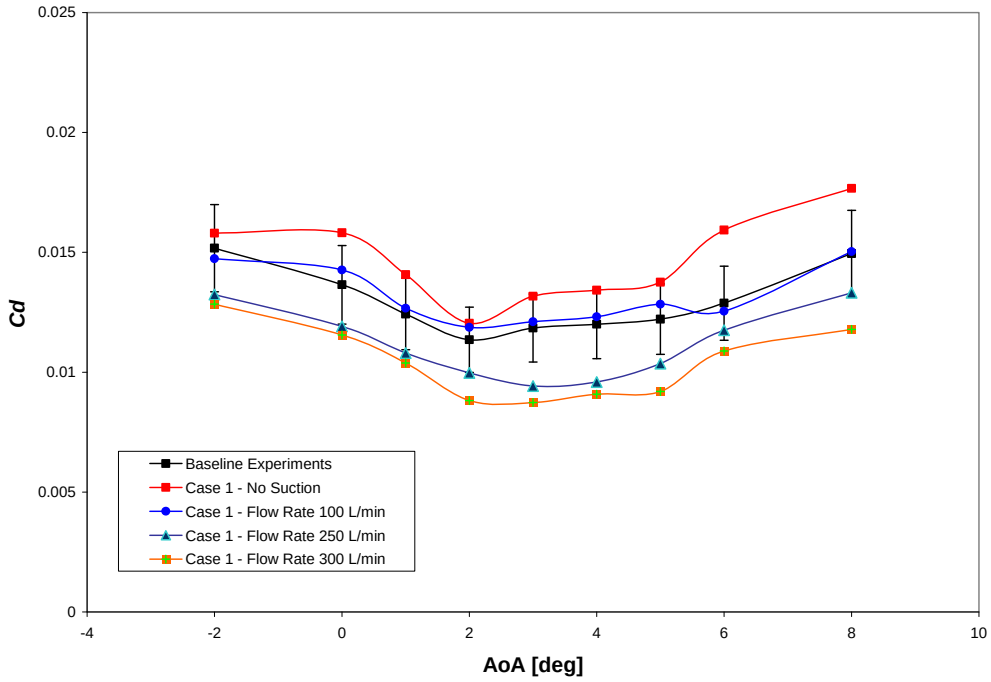


**Figure 19 Comparison of Baseline and Case 1 $C_d$ Results**

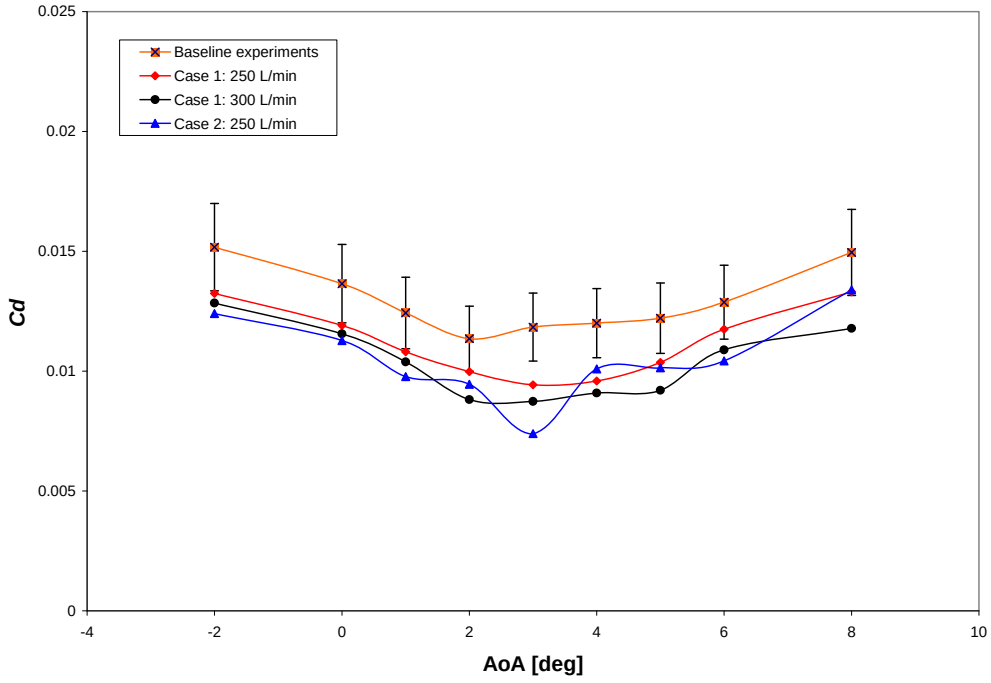


**Figure 20 Comparison of Baseline, Case 1 and Case 2 $C_d$ Results**

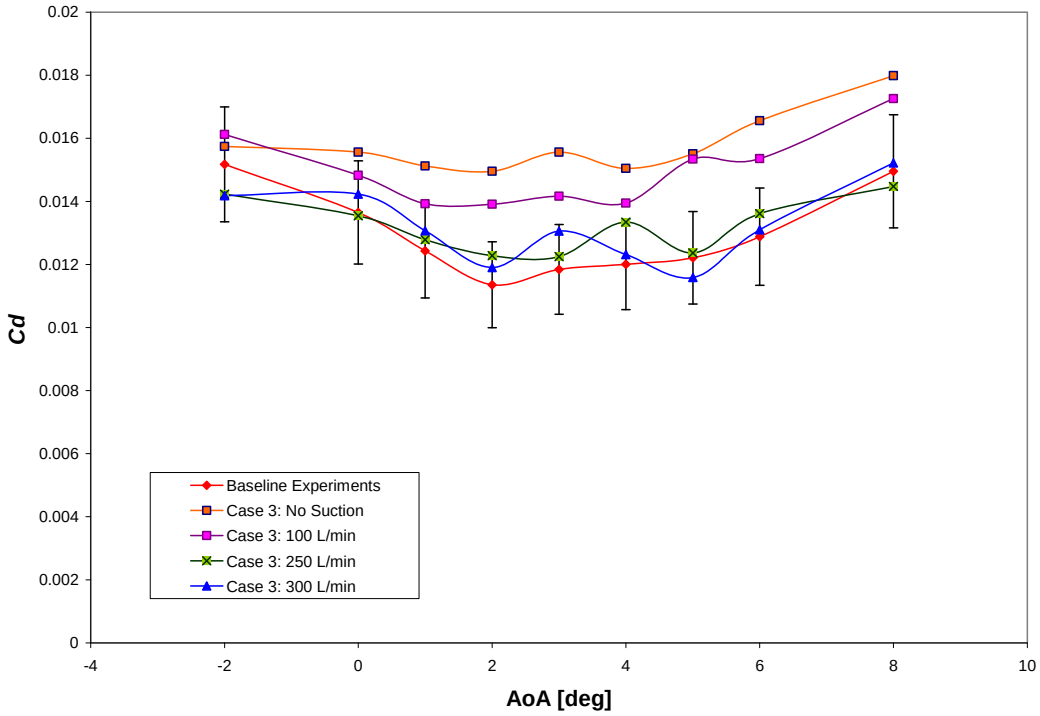


**Figure 21 Comparison of Baseline and Case 3 $C_d$ Results**

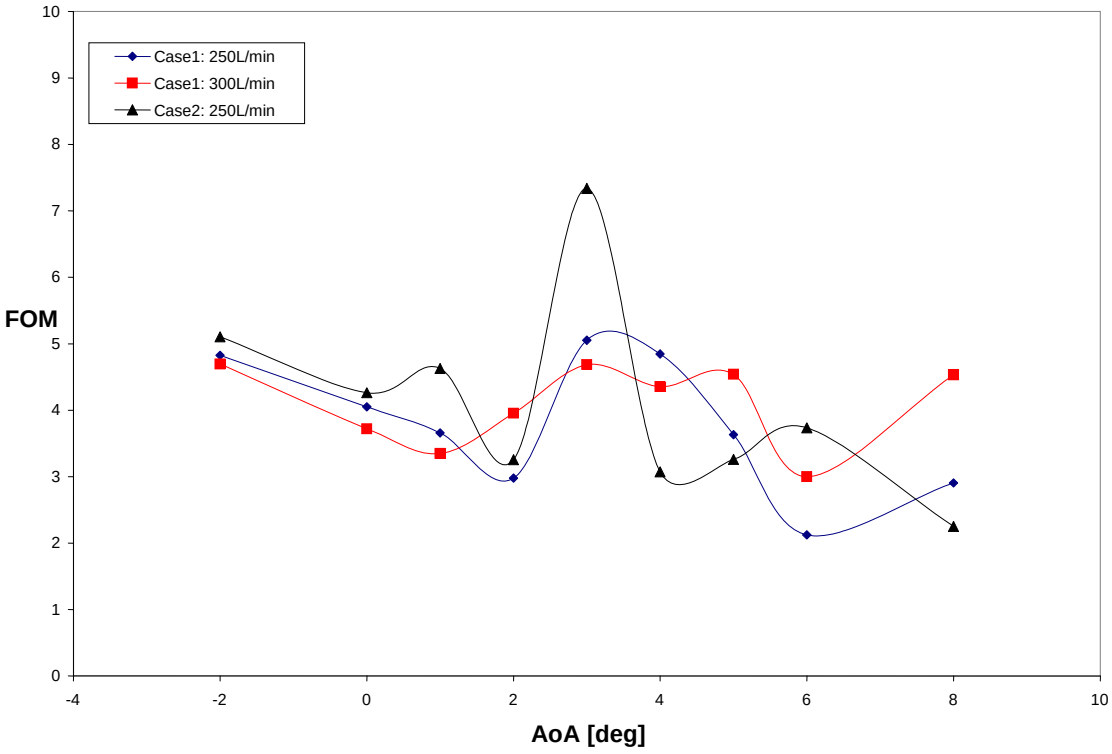


**Figure 22 Variation of FOM with α for Case 1 and Case 2**